Monthly Notices
of the
ROYAL ASTRONOMICAL SOCIETY

Mon. Not. R. Astron. Soc. **415,** 2063–2080 (2011) doi:10.1111/j.1365-2966.2011.18752.x

Stellar population gradients in Fornax cluster S0 galaxies: connecting bulge and disc evolution

A. G. Bedregal,[1,2]★ N. Cardiel,[1] A. Aragón-Salamanca[2] and M. R. Merrifield[2]

[1]*Departamento de Astrofísica, Facultad de Ciencias Físicas, Universidad Complutense de Madrid, 28040 Madrid, Spain*
[2]*School of Physics and Astronomy, University of Nottingham, University Park, Nottingham NG7 2RD*

Accepted 2011 March 18. Received 2011 March 2; in original form 2010 December 6

ABSTRACT

We present absorption-line index gradients for a sample of S0 galaxies in the Fornax cluster. The sample has been selected to span a wide range in galaxy mass, and the deep FORS2 spectroscopy on the VLT allows us to explore the stellar populations all the way to the outer disc-dominated regions of these galaxies. We find that globally, in both bulges and discs, star formation ceased earliest in the most massive systems, as a further manifestation of downsizing. However, within many galaxies, we find an age gradient which indicates that star formation ended first in the outermost regions. Metallicity gradients, when detected, are always negative such that the galaxy centres are more metal-rich. This finding fits with a picture in which star formation continued in the central regions, with enriched material, after it had stopped in the outskirts. Age and metallicity gradients are correlated, suggesting that large differences in star formation history between the inner and outer parts of S0 galaxies yield large differences in their chemical enrichment. In agreement with previous results, we conclude that the radial variations in the stellar populations of S0 galaxies are compatible with the hypothesis that these galaxies are the descendants of spiral galaxies whose star formation has ceased. With the addition of radial gradient information, we are able to show that this shutdown of star formation occurred from the outside inward, with the later star formation in the central regions offering a plausible mechanism for enhancing the bulge light in these systems, as the transformation to more bulge-dominated S0 galaxies requires.

Key words: galaxies: clusters: individual: NGC 1316 – galaxies: clusters: individual: NGC 1380 – galaxies: elliptical and lenticular, cD – galaxies: evolution – galaxies: formation – galaxies: stellar content.

1 INTRODUCTION

In order to better understand the formation and evolution of S0 galaxies, we have undertaken a detailed study of these systems in the Fornax cluster, combining deep optical long-slit spectroscopy obtained with the FORS2 instrument on the VLT with archival optical and near-infrared imaging. The sample and major-axis kinematics of these galaxies are presented in Bedregal et al. (2006a, hereafter Paper I). In Bedregal, Aragón-Salamanca & Merrifield (2006b, hereafter Paper II), we used those data to study the Tully–Fisher relation (Tully & Fisher 1977) for these systems as part of a larger compilation of 60 local S0s, and concluded that their disc kinematics were consistent with what would be expected if these systems were simply faded S0 galaxies. In Bedregal et al. (2008, hereafter Paper III) we studied the central stellar population properties of these galaxies, and found evidence that the bulge-dominated regions of these galaxies had star formation properties that varied systematically with the mass of their host galaxies. In this paper, we seek to tie together these bulge and disc properties by studying the gradients in common absorption-line indices. By obtaining such gradients out as far as the region where the disc dominates the light, and interpreting them in terms of simple stellar population models, we seek an integrated understanding of the formation and evolution of both of the major components of S0 galaxies.

It is already well known that elliptical galaxies and S0 systems show variations in the properties of their stellar populations with radius. Early studies using broad-band colours established that the nuclear regions are usually redder than the outskirts, suggesting radial variations in their stellar population properties (Kormendy & Djorgovski 1989, and references therein). The first study of gradients in spectral absorption features was performed by McClure (1969): in a sample of seven galaxies, he found that an index measuring the central CNλ4216 band strength was stronger than at larger radii, which he interpreted as the result of metallicity variations between the different regions. Subsequent spectroscopic studies, many based on the Lick/IDS line-strength indices (Worthey et al. 1994), have explored absorption feature gradients using a broad range

★E-mail: bedregal@astrax.fis.ucm.es, bedregal@astro.umn.edu

of line indices (e.g. Spinrad 1972; Welch & Forrester 1972; Joly & Andrillat 1973; Cohen 1979; Couture & Hardy 1988; Peletier 1989; Gorgas, Efstathiou & Aragón-Salamanca 1990; Bender & Surma 1992; Davies, Sadler & Peletier 1993; Carollo, Danziger & Buson 1993; González 1993; Fisher, Franx & Illingworth 1995; Gorgas et al. 1997; Mehlert et al. 2003; Sánchez-Blázquez, Gorgas & Cardiel 2006, 2007). Overall, these studies indicate the presence of strong gradients in CN features (at 3883 and 4216 Å), weaker gradients in the Mg-triplet (at ≈5200 Å), *g*-band, Na D lines, Ca H&K features and some Fe I sensitive indices, and no gradients in the hydrogen Balmer series (e.g. Hβ, Hγ), MgH, TiO, Ca I and the infrared Ca triplet. Many of these studies suggest that the existence of gradients in metallic features is produced by radial variations of metallicity, decreasing outwards (e.g. Cohen 1979; Davies et al. 1993; Kobayashi & Arimoto 1999; Mehlert et al. 2003). Other works, however, suggest that there is also a gradient in the stellar population age, the central regions being younger than the outer parts (e.g. Gorgas et al. 1990; Munn 1992; González 1993; González & Gorgas 1996).

These absorption-line index gradients provide clues to the mechanisms responsible of galaxy formation. Chemodynamical models of scenarios such as monolithic collapse, merger-driven evolution and other secular processes predict different gradients. Although quantitative modelling of these effects is still in its infancy, clear qualitative indicators are becoming established. For example, monolithic collapse models (e.g. Eggen, Lynden-Bell & Sandage 1962; Larson 1974a; Carlberg 1984; Arimoto & Yoshii 1987) generically predict the formation of strong gradients for both age- and metallicity-sensitive indices, while, in comparison, a formation history driven by mergers will weaken any such gradients significantly (e.g. White 1980; Bekki & Shioya 1999; Barnes & Hernquist 1991; Mihos & Hernquist 1994).

Clues to the more detailed star formation history of a galaxy can be obtained by comparing individual chemical elements. The different time-scales associated with the supernova producing α-elements (such as Mg) and Fe mean that two galaxies with the same mean stellar age but different histories will display different gradients in these elements. For example, a galaxy in which the stars were produced by a short starburst in the distant past and one where the star formation was over a more extended period may display similar constant Fe index values with radius, but the former will show a decreasing gradient in Mg line strengths while the latter will display a flatter Mg index profile (e.g. Thomas 1999).

Thus, absorption-line index gradients offer a valuable tool in the study of galaxy formation and evolution. Although we are not yet in a position to evaluate such gradients in an unequivocal quantitative manner, their basic interpretation is fairly clear. Even without detailed modelling, their differential use is robust in that systematic differences between galaxies of different types are generally unambiguous. In addition, significant progress is being made with the quantitative analysis of such data, through the development of more sophisticated stellar population models. Hence, the philosophy of this work is initially to make use just of the directly observable line-strength gradients of the Fornax S0s to seek qualitative insight into any systematic variations in their evolutionary histories, and then to go on to use the new stellar population models of Vazdekis et al. (2010) to interpret such results in a more quantitative manner.

The remainder of the paper is as laid out as follows. In Section 2, we present the line index gradients derived from the deep long-slit spectroscopy of nine Fornax cluster S0 galaxies, with the associated detailed plots and values for individual galaxies provided in Appendix A. Section 3 describes the use of the new stellar population models to obtain ages and chemical abundances (and their gradients) from the observed line indices, with the detailed data given in Appendix B. In Section 4, we discuss the implications of the results on the formation history of S0 galaxies, while Section 5 summarizes these results.

2 LINE-STRENGTH INDEX GRADIENTS

In this section, the index gradients measured for 10 common absorption lines are presented. These are the same indices derived for the centres of these galaxies in Paper III, and the details of how they and their associated uncertainties were measured are presented in that paper. A description of how the spectra were binned in the spatial direction is also presented in Paper III (section 2). The binning was designed to yield a minimum signal-to-noise ratio in each spatial bin so that reliable spectral indices could be measured (see Paper III for details). Note that for consistency all indices are calculated on a magnitude scale.

In Appendix A, Figs A1 to A5 show line index measurements along the photometric major axes of the sample galaxies. The radial profiles have been folded around their galaxies' centres to give a sense of any systematic variations. The radii have been scaled to each galaxy's half-light radius (hereafter $R_{\rm HALF}$) as calculated from infrared photometry (in the $K_{\rm s}$ band; see Paper II). The straight lines show linear fits of these logarithmic parameters, with those points lying at radii small enough to be affected by seeing excluded from the fit. The resulting values of the index gradients and their uncertainties are presented in Table A1.

The line index gradients sample different fractions of the bulge- and disc-dominated regions of these galaxies. In Paper I we calculated a limiting radius ($R_{\rm LIM}$, dot–dashed blue lines in Figs A1 to A5) from which the light profile is dominated by the disc component. Therefore, with $R_{\rm LIM}$ we can assess the contribution of each component to the measured gradients. The relative bulge and disc contribution to the gradients is rather heterogeneous among our galaxy sample. For three galaxies the number of radial bins dominated by disc light is less than 30 per cent (NGC 1380, 1381 and 1375). For two other systems the disc contribution is between 70 and 90 per cent (NGC 1380A and IC 1963), while other two galaxies show gradients totally dominated by the disc light (ESO 358-G006 and ESO 359-G002). Finally, NGC 1316 and ESO 358-G059 have no information in this regard as $R_{\rm LIM}$ cannot be estimated in those systems where the disc never dominates the luminosity profiles.

In order to summarize this mass of information and search for systematic variations between Fornax cluster S0s, Fig. 1 shows overplotted the radial variation in all the line indices for all the sample galaxies. The galaxies have been divided and colour-coded by luminosity.

(i) *Bright S0s* ($-19.0 \leq M_{\rm B} \leq -20.6$): NGC 1316, 1380 and 1381, shown as black symbols.

(ii) *Intermediate S0s* ($-18.1 \leq M_{\rm B} \leq -18.5$): NGC 1380A, 1375 and IC 1963, shown as blue symbols.

(iii) *Faint S0s* ($-17.3 \leq M_{\rm B} \leq -17.5$): ESO 358-G059, ESO 358-G006 and ESO 359-G002, shown as red symbols.

When interpreting the results we need to take into consideration that NGC 1316 (in the bright S0 category) shows clear evidence of having suffered a recent merger (Schweizer 1980; Goudfrooij et al. 2001a,b; Paper I), so may not be representative of the class. As is clear from Fig. 1, there are strong variations in behaviour both between different line indices and between different galaxies, but

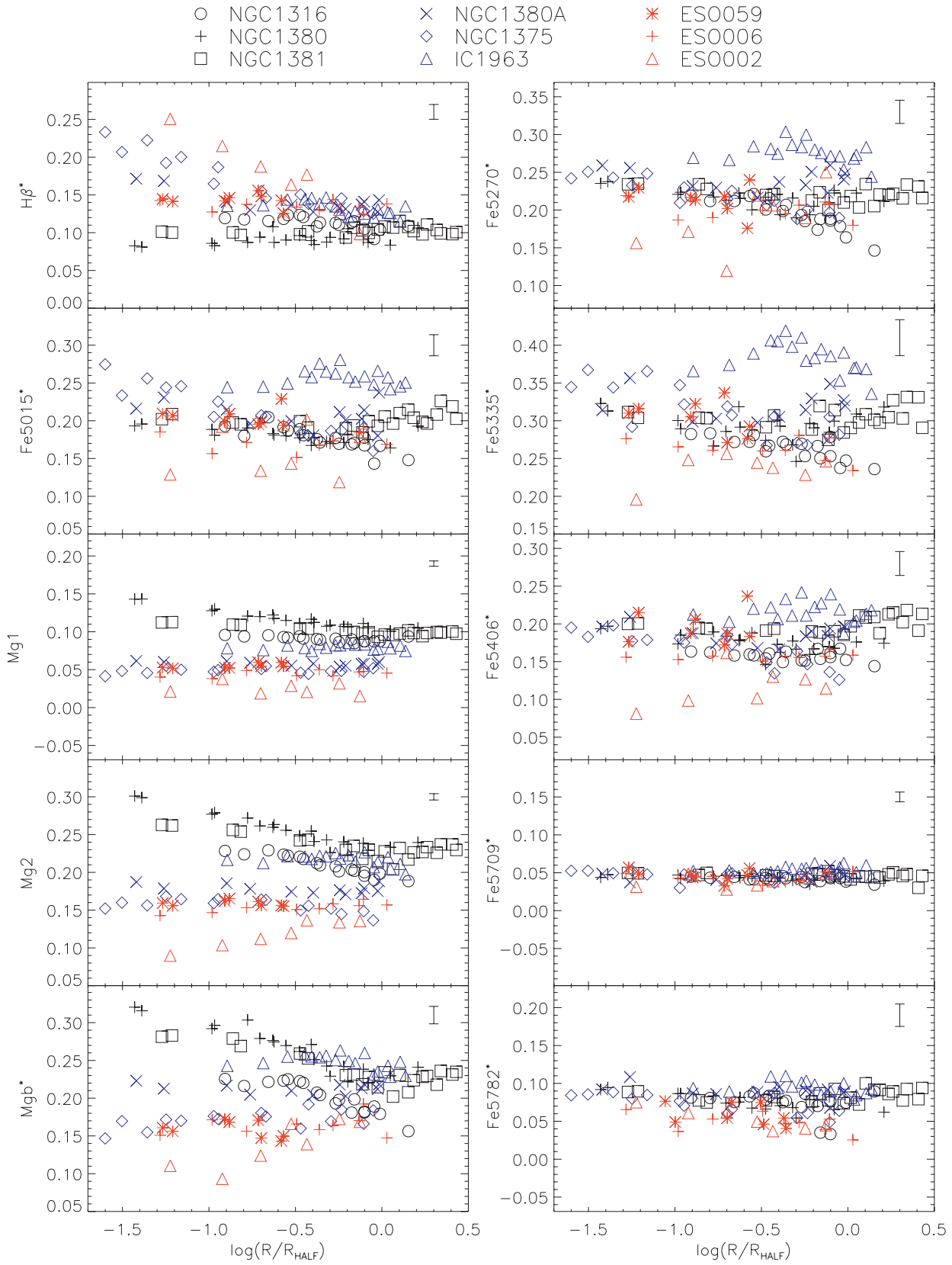

Figure 1. Measurements of 10 line-strength indices as a function of radius for the entire galaxy sample. The key to the symbol representing each galaxy is shown at the top of the figure. The colour code split the galaxy sample by luminosity into a bright (black), intermediate (blue) and faint (red) sample. For clarity, the error bars on each point, shown in the individual profiles of Figs A1–A5, are not shown. Instead, in the top-right corner of each panel we present the median $\pm 1\sigma$ uncertainty of the measured indices.

some systematic trends are immediately apparent. We therefore seek to explore those systematic effects more fully.

One initial point to note is that most of the stronger gradients measured are driven by the inner parts of bulge-dominated regions (e.g. Mg indices in NGC 1380, 1381, Hβ in NGC 1375). Generally, the radial profiles become fairly flat even before reaching 1 $R_{\rm HALF}$, immediately suggesting a scenario in which bulge and disc components may have undergone rather different mass assembly and star formation histories. However, the radial behaviour of the indices present strong variations from galaxy to galaxy, suggesting a degree of variation in any such history. In addition, the different line indices behave in rather different ways: all panels in Fig. 1 have vertical widths of 0.3 mag to allow a fair visual comparison between radial index profiles, and so it is apparent that the Hβ and Mg indices display a wide variety of radial gradients, while the Fe tracers have much flatter profiles, but with a range of absolute values.

Perhaps the most interesting phenomenon is that the Hβ index, while varying widely from galaxy to galaxy at small radii, seems to converge to a common low value at large radii. The lower-mass systems have systematically steeper gradients in this index, and correspondingly higher central values, while the higher-mass galaxies have similar low values of Hβ at all radii. The simplest interpretation of this effect is that the lower-mass galaxies have undergone their final episode of star formation more recently, and that this star formation occurred primarily at small radii. It is possible that the final star formation event in the higher-mass galaxies was similarly centrally concentrated, but occurred sufficiently long ago that any gradient in Hβ has now disappeared. We also need to be a little careful because variations in the Hβ line index arise from both metallicity and age effects. We therefore now turn to interpreting the physical significance of the Hβ profile and those of the other line indices.

3 SINGLE STELLAR POPULATION PARAMETERS AND THEIR GRADIENTS

Given the complex dependency of the observed absorption-line indices on stellar population properties such as star formation history and the chemical abundances of different elements, we rely on somewhat simplified models to translate the observations into parameters that have at least a crude physical interpretation. In particular, by fitting these indices to models of a single stellar population (SSP) with all stars having a common age and chemical abundances, we can derive a luminosity-weighted measure of the age, metallicity and α-abundance of the observed population.

In this section, we will present the steps required to estimate these parameters using the new SSP models of Vazdekis et al. (2010) based on the MILES stellar library (Sánchez-Blázquez et al. 2006; Cenarro et al. 2007). This library, with its $\sim$1000 stellar spectra, provides very good coverage of the stellar atmosphere parameter space (gravity, temperature and metallicity) at a much higher spectral resolution than the original Lick/IDS stellar library: with an instrumental dispersion of $\approx$56 km s^{-1}, it is well matched to the data analysed here, allowing us, in many cases, to use the full observed spectral resolution when comparing data and models. Indeed, the velocity dispersion of the galaxy data implies that in many situations we will be degrading the SSP models to the resolution of the galaxy spectra, and not the other way round, thus minimizing the loss of information. This optimal use of the data is particularly important in the fainter low-mass galaxies and in the disc-dominated outer regions of all the systems, as these regions share the observationally challenging properties of low surface brightness and low intrinsic velocity dispersion. One further benefit of the MILES data is that they are flux calibrated, avoiding the complex and somewhat uncertain corrections involved in placing the absorption-line indices in the Lick/IDS library system. Note that the Mg_1 and Mg_2 indices presented in Paper III were corrected to the Lick/IDS system, but the ones used here are not.

The Vazdekis et al. (2010) models make full use of the MILES library and incorporate the latest developments in stellar evolution and SSP model techniques. In addition, they offer a publicly available easily-usable web-based code (http://miles.iac.es/), which means that the analysis here can readily be reproduced and compared to the results from other data sets, thus making it the ideal choice for this analysis.

3.1 Stellar population parameters

We estimate SSP ages and metallicities ([M/H]) using Vazdekis et al. (2010) model predictions and assuming a Kroupa-Revised initial mass function (IMF; Kroupa & Weidner 2003). The model spectra, corresponding to different combinations of age and [M/H], were matched to the spectral resolution for each galaxy and radial position by convolving them with a Gaussian of dispersion

$$\sigma = \sqrt{\sigma_{\rm gal}^2 - \sigma_{\rm lib}^2}, \quad (1)$$

where $\sigma_{\rm gal}$ is the velocity dispersion of the galaxy at the corresponding radius (see Paper I), and $\sigma_{\rm lib}$ is the resolution from the stellar library. Since $\sigma_{\rm lib}$ has a small, but significant, wavelength dependence, the model spectra were degraded separately for each of the absorption lines used as the main diagnostics (Hβ, Mgb, Fe5270 and Fe5335) using the value appropriate for the central wavelength of each feature. In the cases where $\sigma_{\rm gal} < \sigma_{\rm lib}$ (NGC 1380A, IC 1963, ESO 358-G059, ESO 358-G006 and the outskirts of NGC 1381, NGC 1375 and ESO 359-G002), the galaxy spectra were degraded to reach the library's resolution by convolving them with a Gaussian of dispersion

$$\sigma = \sqrt{\sigma_{\rm lib}^2 - \sigma_{\rm inst}^2 - \sigma_{\rm gal}^2}, \quad (2)$$

where $\sigma_{\rm inst}$ is the FORS2 instrumental dispersion of $\sim$30 km s^{-1}.

Once the model and galaxy spectra were matched in resolution, their line-strength indices were measured. To estimate ages and [M/H], model grids for each individual galaxy data point were created as illustrated by the example shown in Fig. 2. In this figure we show the radial data of NGC 1316 with Vazdekis et al. (2010) SSP model grids for three different metallicity tracers. The colour code of the galaxy data represents the corresponding galactocentric distance. Note that we only show the grids for the models with the largest and smallest velocity dispersions to illustrate the amplitude of this effect; for the actual fitting, each data point was matched to its own grid of models. In the final modelling, the parameters were calculated using Hβ as the main age-sensitive index. Given the range of α-element abundances hinted at by the analysis of Section 2, we adopt the combined [MgFe]$'$ index as the primary measure of [M/H], due to its negligible sensitivity to α-element abundance (González 1993; Thomas, Maraston & Bender 2003). The best estimate SSP values of age and [M/H] were then obtained from this grid using a bivariate polynomial interpolation between the calculated grid values. Finally, any variation with radius in the relative α-element abundances is traced using the Mgb/$\langle$Fe$\rangle$ ratio (see Paper III and fig. 4 of Thomas et al. 2003). The resulting profiles for age, [M/H] and α-enhancement with radius for all of the sample galaxies are presented in Appendix B (Figs B1–B5).

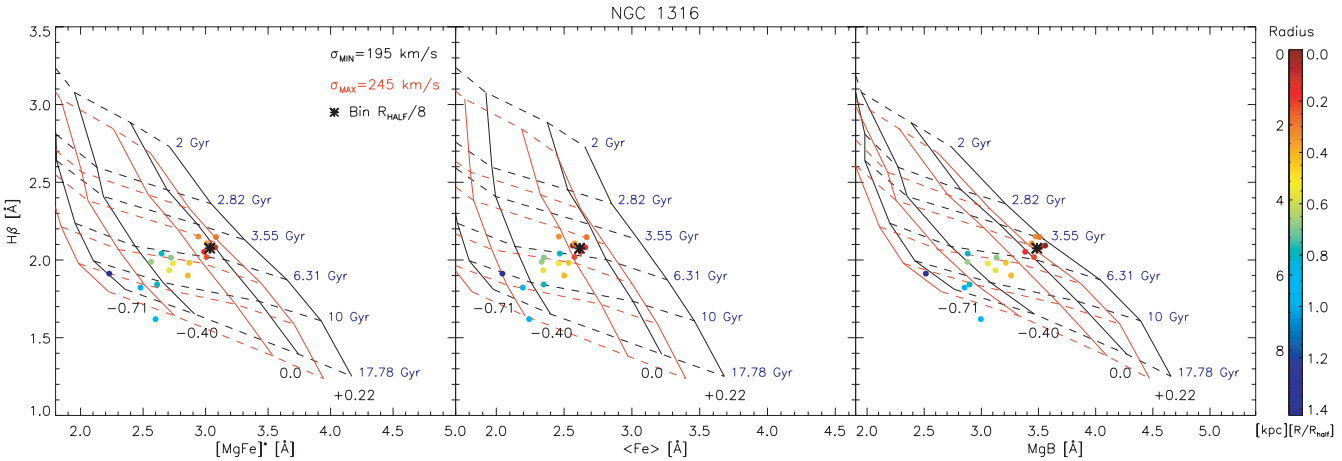

Figure 2. Example of NGC 1316 radial data with Vazdekis et al. (2010) SSP model grids. Hβ is used as the age-sensitive index, while [MgFe]$'$ (left), $\langle$Fe$\rangle$ (centre) and Mg*b* (right) are used as [M/H]-sensitive indicators. Colour code on galaxy data represent the radial distance of each data point. The black asterisks represent the central measurements (within $R_{\rm HALF}/8$). For clarity, only two model grids are shown, those with the higher (red) and lower (black) galaxy velocity dispersion.

3.2 Uncertainties

When interpreting any correlations apparent in these results, it is important to realize that the nature of the modelling process means that the estimated parameters are not independent. We must therefore take some care in estimating the associated uncertainties. The errors in individual data points were calculated by Monte Carlo simulation, generating pairs of values around the measured Hβ and [MgFe]$'$ indices, with a dispersion matched to the observational errors on these quantities, placing them on the model grid, and then extracting the age and [M/H] parameters. The 68th percentile of the resulting age and [M/H] distributions then provides a realistic quasi-elliptical 1σ error contour around the derived age–[M/H] value. The associated (often asymmetric) error bars can then be derived by projecting the error contours on to the age and [M/H] axes.

Similarly, the uncertainties in the Mg*b*/$\langle$Fe$\rangle$ ratio (our α-abundance tracer) were estimated by Monte Carlo simulations, producing symmetric error bars in this case.

3.3 Gradients

Figs B1–B5 in Appendix B show the radial variation of the derived ages, [M/H] and α-enhancement indicators for all the galaxies, together with their uncertainties. Linear fits to those gradients are plotted as solid lines. The slopes of these fits (hereafter called 'gradients') are given in Table B1.

The uncertainties in age and [M/H] gradients were calculated using the Monte Carlo simulations described above for every Hβ-[MgFe]$'$ pair, translated into simulated age–[M/H] pairs. From these values we created a large number of realizations of the radial distributions of these two parameters for every galaxy, each of which was fitted with a linear function to give an estimate of the uncertainty in each gradient (and its correlation with other parameters). The quoted errors in these two parameters are asymmetric as a consequence of using individual age and [M/H] predictions having asymmetric uncertainties (see Section 3.2). Errors in the α-enhancement gradients, also calculated via Monte Carlo simulations, are symmetric since no models are involved in their determination.

4 RESULTS

There are almost no previous studies of the stellar population gradients in S0s where these galaxies are treated as a separate class from the ellipticals (hereafter Es). The work of Fisher, Franx & Illingworth (1996) is one of the few exceptions. For a sample of nine bright edge-on S0s they found that their bulge and disc metallicity gradients differ substantially, being steep and decreasing outwards in the bulge region while becoming flat in the stellar disc. They also found that the central Mg and Fe indices correlate with central velocity dispersion (hereafter σ_0) as in luminous Es. Hence, they conclude that S0 bulges are probably the result of a dissipative collapse process (such as gas-rich mergers) at very early times.

For a combined sample of 35 E and S0 galaxies in the Coma cluster, Mehlert et al. (2003) calculate gradients reaching $\approx 1 R_{\rm HALF}$. They found that Es have on average slightly higher velocity dispersions, lower Hβ and higher metallic line strengths than S0s. The latter form two families, one comparable to the Es and a second one with much younger stellar populations ($\sim$2 Gyr), and weaker metallic lines. This result was later confirmed by Kuntschner et al. (2006) within the SAURON collaboration (Bacon et al. 2001). These authors studied a sample of 48 local Es and S0s and identified the young, low-σ_0 S0s as the main drivers of the observed trends between gradients and central line indices.

In the light of these results we now analyse the gradients found in our Fornax S0 sample. The first point apparent from Table B1 is that virtually all the age gradients are positive or flat, indicating that the star formation ended first in the disc-dominated outer regions of the galaxies. This result confirms the qualitative indication that we found from the Hβ gradients shown in Fig. 1. Indications of this result were also found in Paper II, and we argued there that centrally concentrated star formation at later times, enhancing the bulge-to-disc ratio, is probably an integral stage in the morphological transformation of a spiral into an S0 galaxy (Christlein & Zabludoff 2004; Shioya, Bekki & Couch 2004). Other observational evidence in favour of this scenario has been presented in the past (Moss & Whittle 2000; Mehlert et al. 2003; Poggianti et al. 2001; Bamford, Milvang-Jensen & Aragón-Salamanca 2007). What is still unclear is whether this late central star formation represents an enhancement over the 'quiescent spiral' star formation rate (perhaps fuelled by

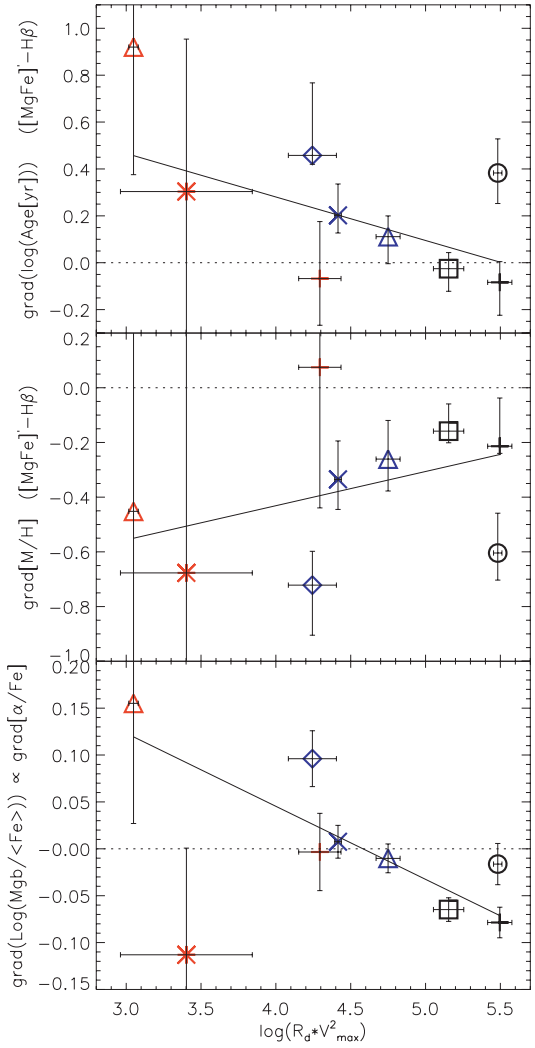

Figure 3. Gradients in age, [M/H] and [α/Fe] tracer versus $\log(R_{\rm d}v^2_{\rm max})$, a proxy for dynamical mass (see Paper III). Continuous lines correspond to best linear fits. Dashed lines represent flat gradients. Symbols as in Fig. 1.

interaction-induced inward gas flows) or is just the last remaining centrally concentrated star formation gasp. The second hypothesis is probably favoured by some recent results (e.g. Wolf et al. 2009) but the evidence is still inconclusive.

Fig. 1 also suggested that the cessation of star formation happened at earlier times in the brightest galaxies, considerably reducing the Hβ and age gradients. If that trend is a reflection of an underlying galaxy mass dependency we would expect an anti-correlation between age gradient and galaxy mass. To test for this effect, Fig. 3 shows the various gradients plotted against $R_d \times v^2_{\rm max}$, which provides a measure of each galaxy's mass (see Paper III). There does seem to be a trend between age gradient and mass in the sense described (a Spearman rank test gives a probability of correlation between 95 and 97.5 per cent), although NGC 1316, whose central regions have probably been rejuvenated by a recent merger, seems to deviate somewhat. Possible correlations between the gradients in [M/H] or α-enhancement and galaxy mass are either weaker or not detected (Spearman rank tests give <90 per cent and 90–95 per cent probabilities, respectively). Previous studies (Mehlert et al. 2003; Rawle, Smith & Lucey 2010) found no correlations between these parameters in early-type galaxies (although see Spolaor et al. 2009 and Kuntschner et al. 2010 at low masses). In any case, some care is necessary in not overinterpreting these trends (or lack thereof) given the limitations imposed by the sample size and uncertainties.

Close inspection of Figs B1 to B5 also reveals that the generally old age that we had ascribed to the discs in Section 2 is not the whole story, in that the age in the outer disc-dominated regions is $\gtrsim$10 Gyr for the brightest and most massive galaxies, while it is only $\simeq$4–5 Gyr for the less massive ones. This would seem to be a new manifestation of 'downsizing': star formation stopped first in the most massive galaxies not only in their centres [as found before in other early-type galaxy samples; see Smith, Lucey & Hudson (2009) and references therein] but also in their oldest outermost regions.

In Paper III we reported a tentative correlation between the α-element overabundance and age in the central regions of these galaxies. This correlation is confirmed here with the improved models. A Spearman rank test gives a probability of correlation between 95 and 97.5 per cent (see Fig. 4, top-central panel). The correlation can be explained by considering a simple model where all galaxies started forming stars at approximately the same time, formed stars for different time intervals Δt, and then ceased their star formation t Gyr ago. Since the SSP ages are correlated with t, while the α-element overabundance is anti-correlated with Δt, it follows that the ages must be correlated with the α-element overabundance, as observed (see Paper III and Aragón-Salamanca 2008 for details). Fig. 4 also confirms Paper III finding that there is no correlation between central ages and central [M/H], nor between central [M/H] and central α-enhancements.

When detected, the [M/H] gradients are always negative, implying that the stars in the inner regions of the galaxies are on average more metal-enriched than those in the outskirts. This finding fits in with the growing picture that star formation continued, with enriched material, in the central regions after it had stopped in the outskirts.

Gradients in the α-element enhancement tracer are usually flat within the uncertainties except for the two old and bright S0s (NGC 1380, 1381). These galaxies show clear negative gradients (Table B1). In the bottom-central panel of Fig. 4 we see a trend between Grad(Age) and Grad(α). This trend is consistent with the similar correlation found for the central values (a Spearman rank test gives a 90–95 per cent probability of correlation).

Finally, the top-left panel of Fig. 4 clearly shows that gradients in age and [M/H] are correlated for the six brightest galaxies (black and blue points). Nothing can be said for the faintest three, since no gradients were detected in them within the large errors (see Table B1). A Spearman rank test gives a 99.5 per cent probability of correlation for all nine S0s.

It could be argued that, at least in part, this trend is driven by correlated errors as the 1 σ error ellipses in Fig. 4 are clearly aligned with this trend. We have tested whether this correlation can be totally explained by the observed uncertainties using 10^4 Monte Carlo simulations which consider the observed data points and their error distributions. Using a Kolmogorov–Smirnov test with $\alpha = 0.05$ confidence level we find that 93 per cent of the simulations reject the null hypothesis that our original sample and each simulated one were drawn from the same distribution. This indicates that, although there is a sizable correlation in the errors, there is a real correlation between Grad[M/H] and Grad(Age).

The best linear fit to the Grad(Age) versus Grad[M/H] trend produces a slope of -1.14 ± 0.30. This result is comparable with findings of Sánchez-Blázquez et al. (2007; -1.33 ± 0.37). However, other works on early-type galaxy samples give somewhat different

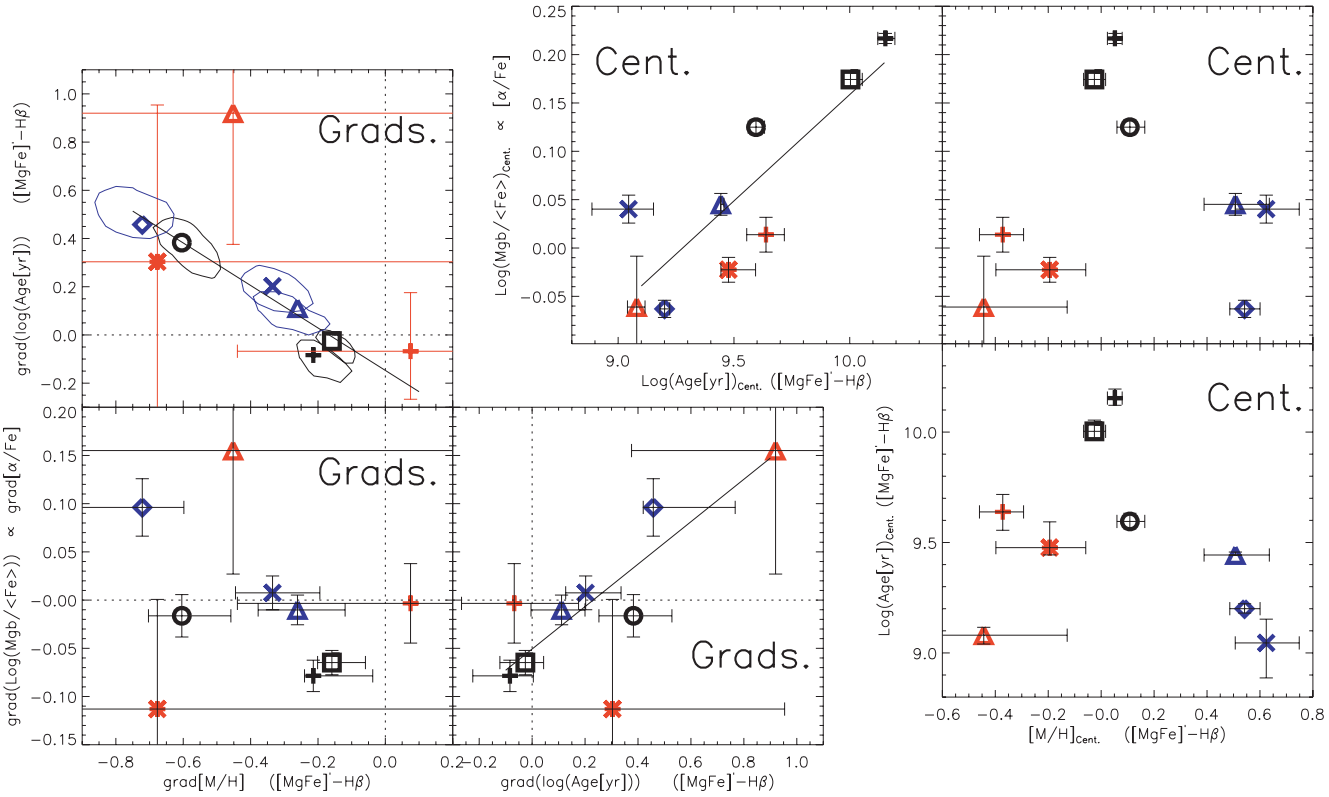

Figure 4. Gradients in age, [M/H] and α-enhancement tracer versus each other and Central age, [M/H] and α-enhancement tracer versus each other. Symbols as in Fig. 1. Continuous lines correspond to the best linear fits. Dashed lines correspond to flat gradients. In Grad(Age) versus Grad[M/H] (top-left panel), errors as 1σ contours have been drown for some galaxies.

results, like Mehlert et al. (2003; -0.95 ± 0.11) and Rawle et al. (2010; -0.69 ± 0.10). The concordance with the Sánchez-Blázquez et al. result might be attributed to the fact that their sample, like ours, has an important fraction of discy, low-σ_0 galaxies. Although difficult to interpret in detail, this correlation indicates that large differences in star formation history between the inner and outer parts of galaxies yield large differences in chemical enrichment, which in retrospect is perhaps not so surprising.

5 SUMMARY

Using deep VLT-FORS2 spectroscopy we have derived absorption-line index gradients for a sample of S0 galaxies in the Fornax cluster spanning a wide range in galaxy mass. Combining these observations with the latest spectral synthesis models (Vazdekis et al. 2010), we have studied the properties of the stellar populations in these galaxies as a function of galactocentric distance, reaching the outer disc-dominated regions.

Our main conclusions are as follows.

(i) The age gradients are positive or flat, indicating that the star formation ended first in the disc-dominated outer regions of the galaxies. This centrally concentrated star formation at later times could serve to enhance the bulge-to-disc ratios of these systems, helping the morphological transformation of spirals into S0s.

(ii) The cessation of star formation in the central regions happened at earlier times in the brightest galaxies, considerably reducing their Hβ and age gradients.

(iii) The age in the outer disc-dominated regions is $\gtrsim$10 Gyr for the brightest and most massive galaxies and $\simeq$4–5 Gyr for the least massive ones. Thus, star formation stopped first in the most massive galaxies not only in their centres but also in their oldest outermost regions, suggesting that 'downsizing' is a rather universal phenomenon.

(iv) Metallicity gradients, when detected, are always negative, such that the galaxy centres are more metal-rich. This result fits with a picture in which star formation continued in the central regions, with enriched material, after it had stopped in the outskirts.

(v) For the brightest galaxies, gradients in age and metallicity are anti-correlated. This trend cannot be attributed to correlated errors. It indicates that large differences in star formation history between the inner and outer parts of S0 galaxies yield large differences in chemical enrichment.

In combination with the previous results obtained in this study (Papers I, II and III), a coherent picture is emerging in which S0 galaxies can be interpreted as spiral galaxies in which star formation has ceased. This conversion process seems to have occurred earliest in the most massive galaxies as a further manifestation of downsizing. What we have been able to add by studying the radial gradients in these systems is the evidence that this cessation happened first in the discs of these systems, with star formation shutting down from the outside inward. Such a sequence fits well with the requirement for a process that enhances the central bulges of S0s relative to their discs when compared to unquenched spiral systems.

ACKNOWLEDGMENTS

This work was based on observations made with European Southern Observatory (ESO) telescopes at Paranal Observatory under programme ID 070.A-0332. This publication makes use of data

products from the Two Micron All Sky Survey, which is a joint project of the University of Massachusetts and the Infrared Processing and Analysis Center/California Institute of Technology, funded by the National Aeronautics and Space Administration and the National Science Foundation. This work has been supported by the Programa Nacional de Astronomía y Astrofísica of the Spanish Ministry of Science and Innovation under grants AYA2007-67752-C03-03 and AYA2006-15698-C02-02.

REFERENCES

Aragón-Salamanca A., 2008, in Bureau M., Athanassoula A., Barbuy B., eds, Proc. IAU Symp. 245, Formation and Evolution of Galaxy Bulges. Cambridge Univ. Press, Cambridge, p. 285
Arimoto N., Yoshii Y., 1987, A&A, 173, 23
Bacon R. et al., 2001, MNRAS, 326, 23
Bamford S. P., Milvang-Jensen B., Aragón-Salamanca A., 2007, MNRAS, 378, L6
Barnes J. E., Hernquist L. E., 1991, ApJ, 370, 65
Bedregal A. G., Aragón-Salamanca A., Merrifield M. R., Milvang-Jensen B., 2006a, MNRAS, 371, 1912 (Paper I)
Bedregal A. G., Aragón-Salamanca A., Merrifield M. R., 2006b, MNRAS, 373, 1125 (Paper II)
Bedregal A. G., Aragón-Salamanca A., Merrifield M. R., Cardiel N., 2008, MNRAS, 387, 660 (Paper III)
Bekki K., Shioya Y., 1999, ApJ, 513, 108
Bender R., Surma P., 1992, A&A, 258, 250
Carlberg R. G., 1984, ApJ, 286, 403
Carollo C. M., Danziger I. J., Buson L., 1993, MNRAS, 265, 553
Cenarro A. J. et al., 2007, MNRAS, 374, 664
Christlein D., Zabludoff A. I., 2004, ApJ, 616, 192
Cohen J. G., 1979, ApJ, 228, 405
Couture J., Hardy E., 1988, AJ, 96, 867
Davies R. L., Sadler E. M. S., Peletier R. F., 1993, MNRAS, 262, 650
Eggen O. J., Lynden Bell D., Sandage A. R., 1962, ApJ, 136, 748
Fisher D., Franx M., Illingworth G., 1995, ApJ, 448, 119
Fisher D., Franx M., Illingworth G., 1996, ApJ, 459, 110
González J. J., 1993, PhD thesis, Univ. California, Santa Cruz
González J. J., Gorgas J., 1996, in Buzzoni A., Renzini A., eds, ASP Conf. Ser. Vol. 86, Fresh Views of Elliptical Galaxies. Astron. Soc. Pac., San Francisco, p. 225
Gorgas J., Efstathiou G., Aragón-Salamanca A., 1990, MNRAS, 245, 217
Gorgas J., Pedraz S., Guzmán R., Cardiel N. González J. J., 1997, ApJ, 481, L19
Goudfrooij P., Alonso M. V., Maraston C., Minniti D., 2001a, MNRAS, 328, 237
Goudfrooij P., Mack J., Kissler-Patig M., Meylan G., Minniti D., 2001b, MNRAS, 322, 643
Joly M., Andrillat Y., 1973, A&A, 26, 95
Kobayashi C., Arimoto N., 1999, ApJ, 527, 573
Kormendy J., Djorgovski S., 1989, ARA&A, 27, 235
Kroupa P., Weidner C., 2003, ApJ, 598, 1076
Kuntschner H. et al., 2006, MNRAS, 369, 497
Kuntschner H. et al., 2010, MNRAS, 408, 97
Larson R. B., 1974a, MNRAS, 166, 585L
McClure R. D., 1969, AJ, 74, 50
Mehlert D., Thomas D., Saglia R. P., Bender R., Wegner G., 2003, A&A, 407, 423
Mihos J. Ch., Hernquist L., 1994, ApJ, 425, L13
Moss C., Whittle M., 2000, MNRAS, 317, 667
Munn J. A., 1992, ApJ, 399, 444
Peletier R. F., 1989, PhD thesis, Univ. Groningen, the Netherlands
Poggianti B. M. et al., 2001, ApJ, 563, 118
Rawle T. D., Smith R. J., Lucey J. R., 2010, MNRAS, 401, 852
Sánchez-Blázquez P., Gorgas J., Cardiel N., 2006, A&A, 457, 823
Sánchez-Blázquez P., Forbes D. A., Strader J., Brodie J., Proctor R., 2007, MNRAS, 377, 759
Schweizer F., 1980, ApJ, 237, 303
Shioya Y., Bekki K., Couch W. J., 2004, ApJ, 601, 654
Smith R. J., Lucey J. R., Hudson M. J., 2009, MNRAS, 400, 1690
Spinrad H., 1972, ApJ, 177, 285
Spolaor M., Proctor R. N., Forbes D. A., Couch W. J., 2009, ApJ, 691, L138
Thomas D., 1999, MNRAS, 306, 655
Thomas D., Maraston C., Bender R., 2003, MNRAS, 339, 897
Tully R. B., Fisher J. R., 1977, A&A, 54, 661
Vazdekis A., Sánchez-Blázquez P., Falcón-Barroso J., Cenarro A. J., Beasley M. A., Cardiel N., Gorgas J., Peletier R. F., 2010, MNRAS, 404, 1639
Welch G. A., Forrester W. T., 1972, AJ, 77, 333
White S. D. M., 1980, MNRAS, 191, 1
Wolf C., et al.2009, MNRAS, 393, 1302
Worthey G., Faber S. M., González J. J., Burstein D., 1994, ApJS, 94, 687

APPENDIX A: LINE INDEX GRADIENTS

In Figs A1–A5, radial measurements (along the semimajor axes) for 10 line indices are presented for the galaxy sample. The radii are scaled to the total galaxy half-light radius ($R_{\rm HALF}$) as calculated from $K_{\rm s}$-band photometry. The radial profiles were folded around the galaxy centre (open and filled symbols; see each figure for details). Linear fits are shown for the radial index profiles (indices in magnitudes) with those points lying in the central region affected by seeing excluded from the fit. The vertical lines show different radial scales for each galaxy when available. The dashed lines (in green) mark the bulge effective radius ($1R_{\rm e}$). The vertical continuous lines (in red) mark the disc scale-length ($1R_{\rm d}$). The dot–dashed lines (in blue) correspond to the radius ($R_{\rm LIM}$) from which the light profile is dominated by the disc component as calculated in Paper I. When $R_{\rm LIM}$ is accompanied by horizontal arrows, it indicates that the line position is indicative only as its real location is too close to the galaxy centre to be shown. The resulting values of the index gradients and their uncertainties are presented in Table A1.

APPENDIX B: SSP PARAMETERS

Figs B1–B5 show SSP ages and [M/H] derived using Vazdekis et al. (2010) models, and the α-element abundance tracer (Mgb/$\langle$Fe$\rangle$ ratio). The notation 'log (Age[yr]) ([MgFe]$'$ – Hβ)' and '[M/H] ([MgFe]$'$ – Hβ)' are used to make explicit the fact that age and [M/H] have been derived using [MgFe]$'$–Hβ diagrams such as the one in Fig. 2 (left-hand panel). The solid lines (in black) show the best linear fits to the radial profiles. The slopes of these fits and corresponding errors are given in Table B1.

The horizontal dashed lines in [M/H] plots represent solar metallicity. The two horizontal dashed lines in the [α/Fe]-tracer plots delimit the log(Mgb/$\langle$Fe$\rangle$) range corresponding to [α/Fe] = 0 [for metallicities $-1.35 \leq$ [Z/H] ≤ 0.35 and ages between $3 \leq t \leq 15$ Gyr according to Thomas, Maraston & Bender (2003) models; for NGC 1380 and 1381 the range is limited to models of ages between $8 \leq t \leq 15$ Gyr]. Horizontal lines as in Figs A1–A5.

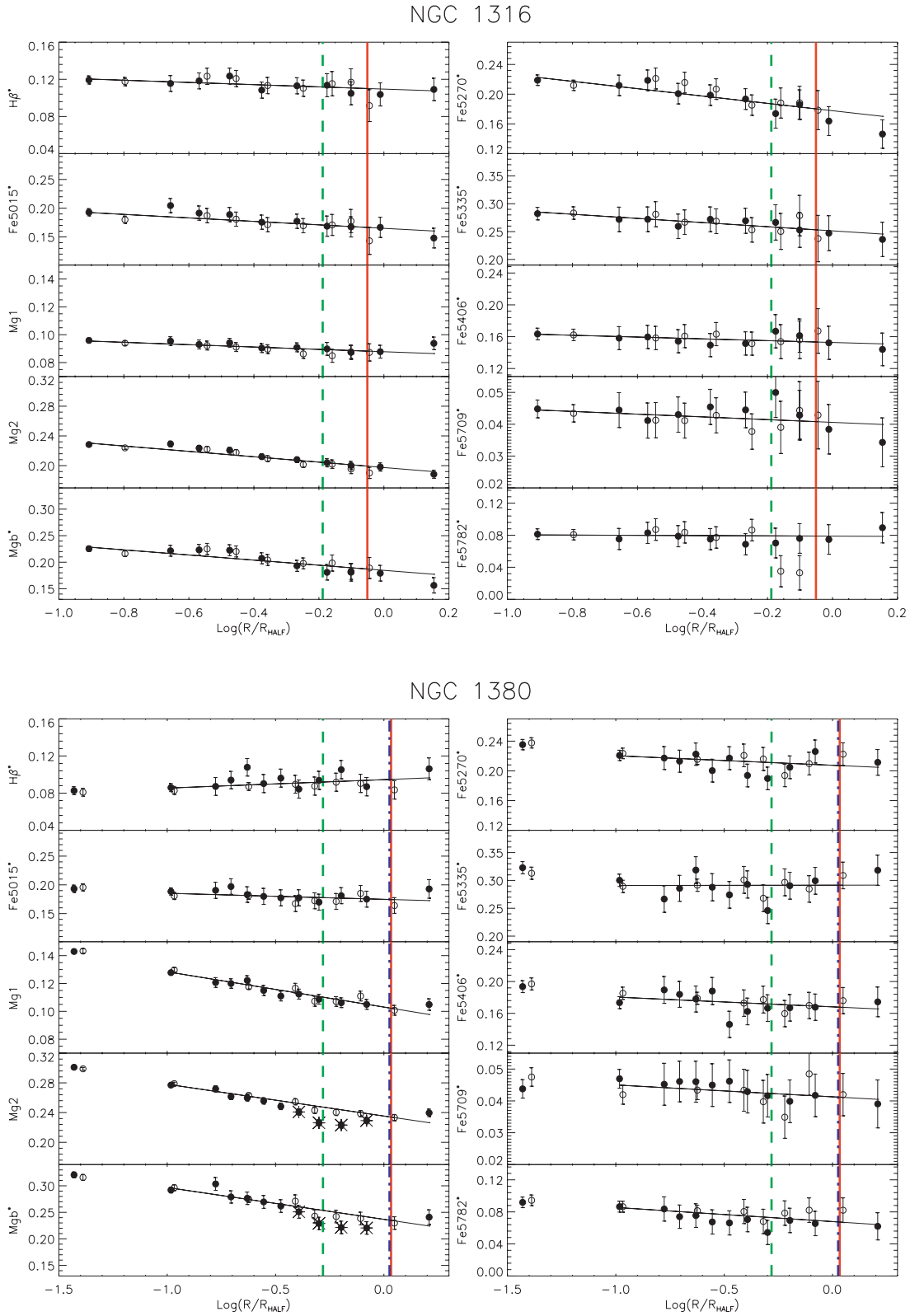

Figure A1. 10 index gradients along the semimajor axis of NGC 1316 and NGC 1380. Filled (open) symbols correspond to: SW (NE) (for NGC 1316) and S (N) (for NGC 1380). Central bin indices are not shown. Linear fits (error-weighted gradients) are shown for the radial index profiles where points within seeing-size from the nucleus were not used. Points with '*' symbols in Mg_2 and Mg*b* indices were not used in the fit as they lie in a bad-pixel area of the detector. See the Appendix text for a description of the vertical lines.

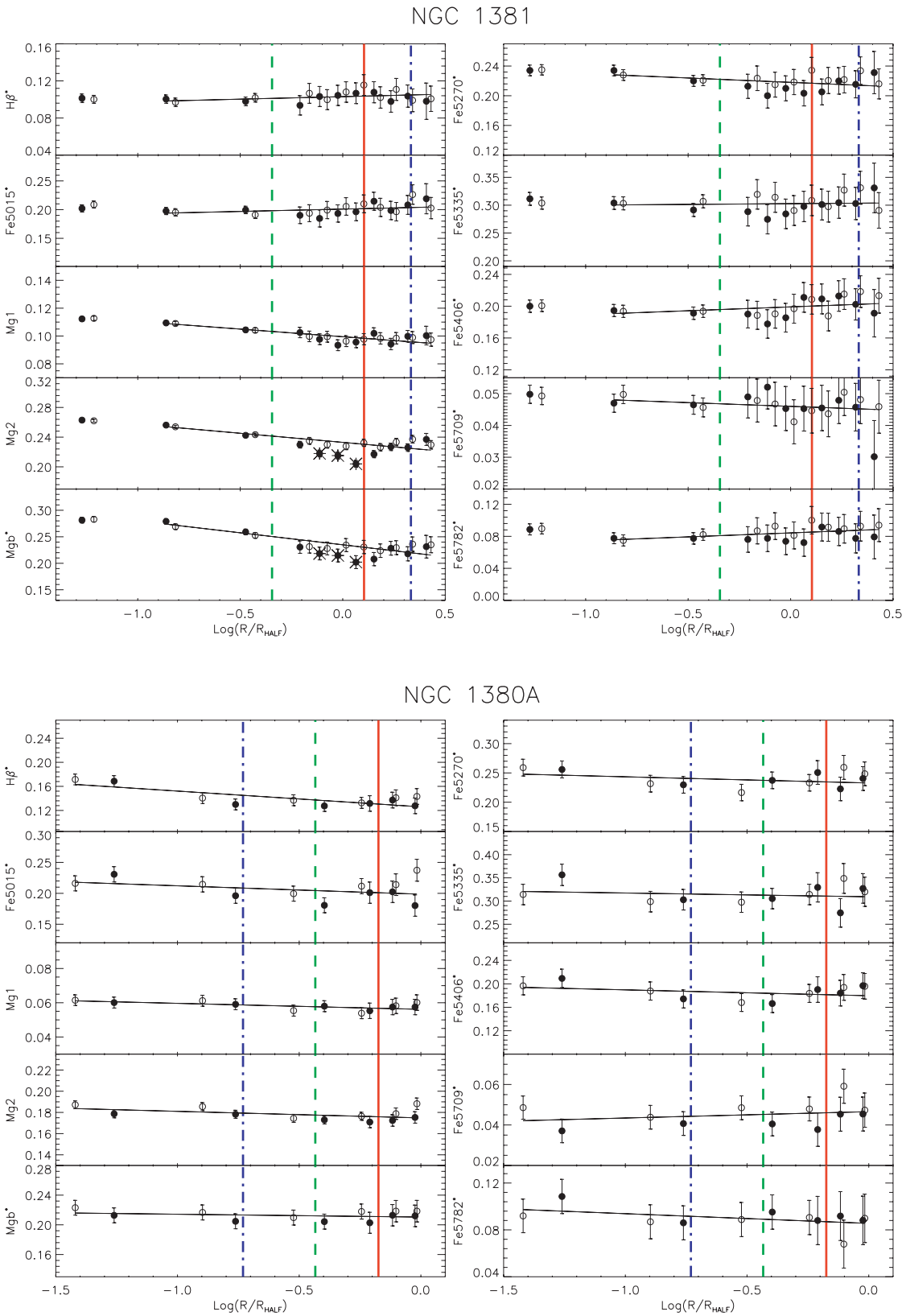

Figure A2. Same as Fig. A1 for NGC 1381 and NGC 1380A. Filled (open) symbols correspond to SE (NW) (for NGC 1381) and S (N) (for NGC 1380A). Points with '*' symbols in Mg_2 and M*gb* indices were not used in the fit as they lie in a bad-pixel area of the detector.

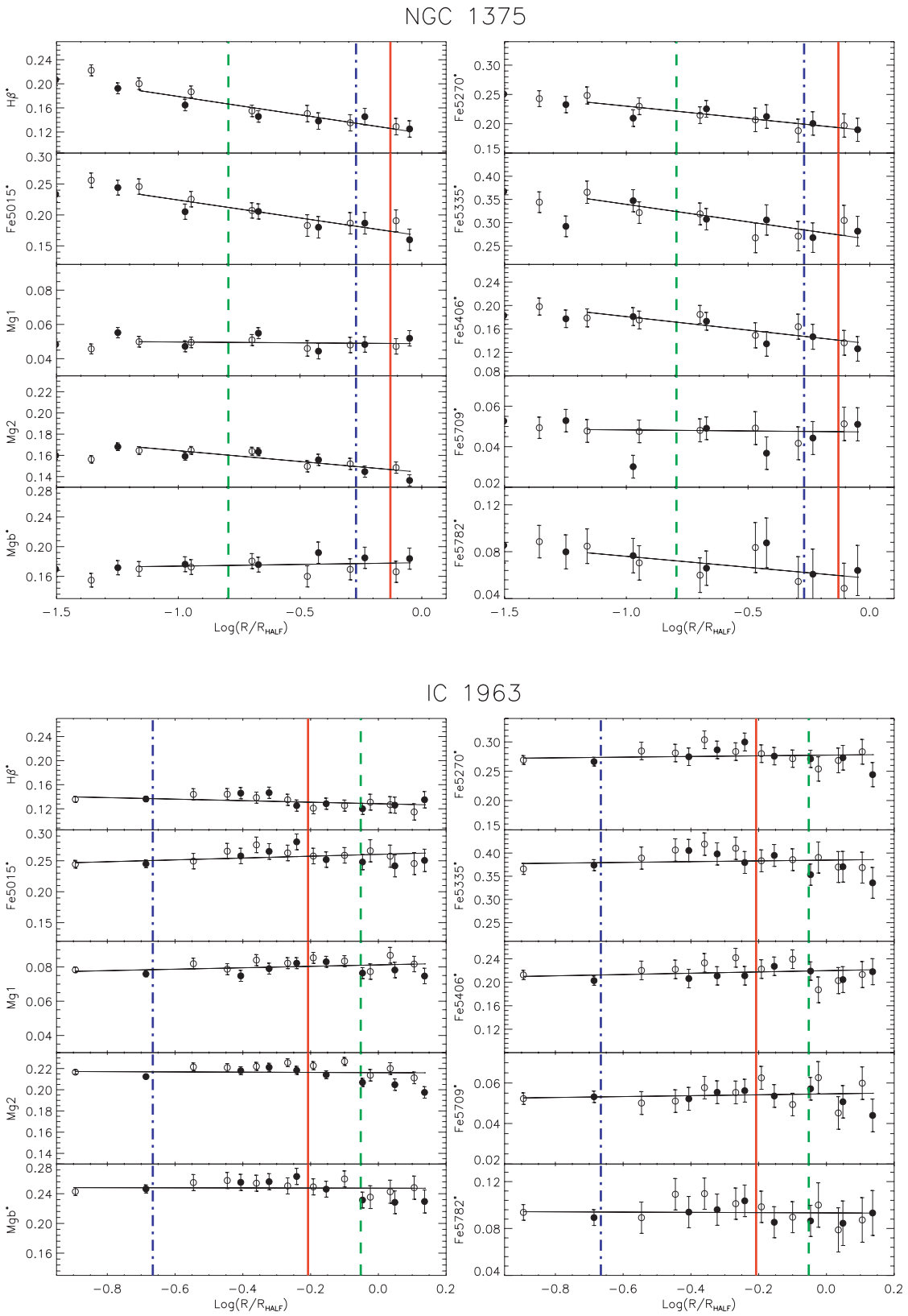

Figure A3. Same as Fig. A1 for NGC 1375 and IC 1963. Filled (open) symbols correspond to: the W (E) profile projected in the sky (for both galaxies).

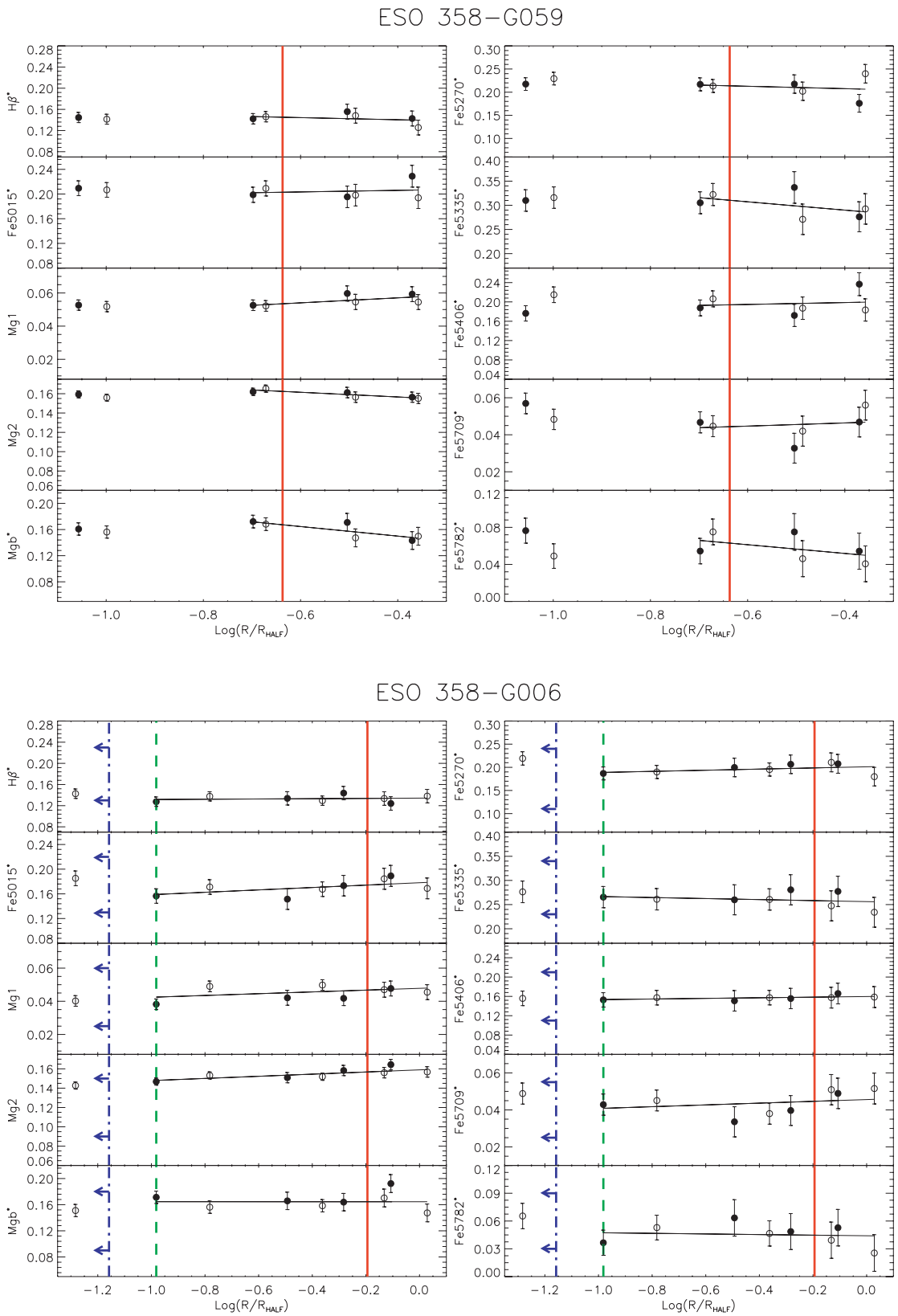

Figure A4. Same as Fig. A1 for ESO 358-G059 and ESO 358-G006. Filled (open) symbols correspond to the SE (NW) (for ESO 358-G059) and SW (NE) (for ESO 358-G006).

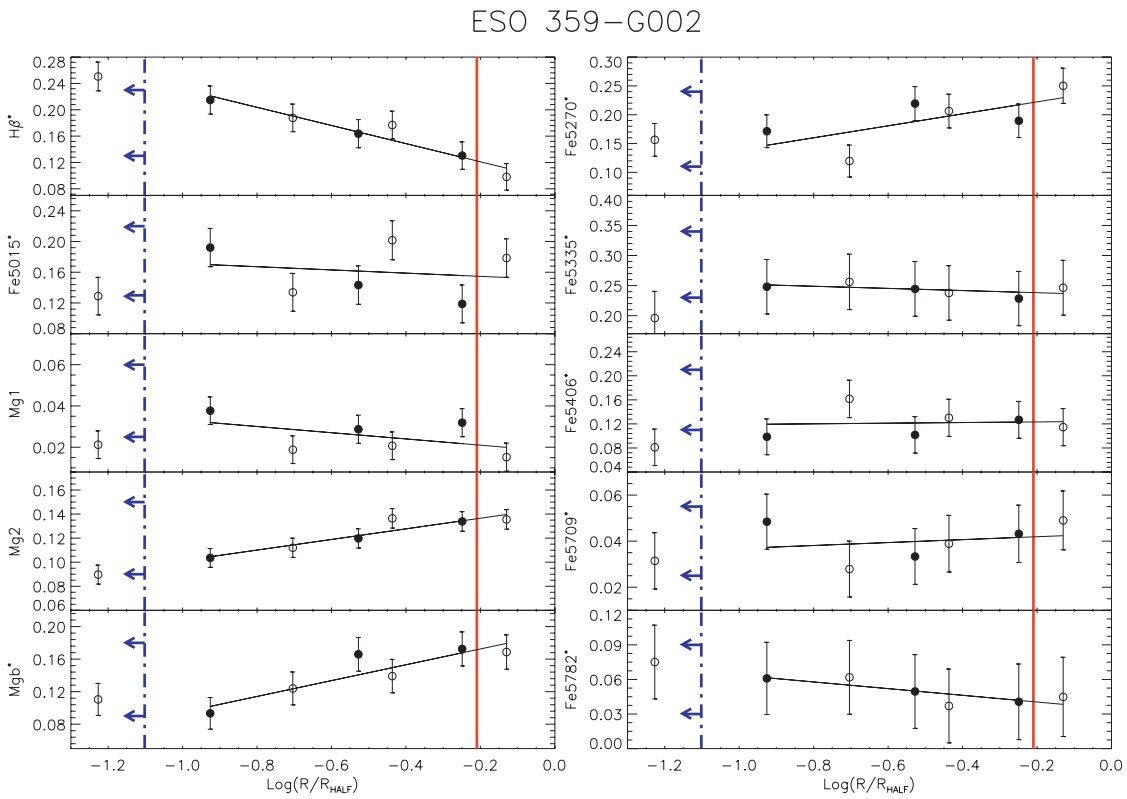

Figure A5. Same as Fig. A1 for ESO 359-G002. Filled (open) symbols correspond to the SW (NE) profile projected in the sky.

Table A1. Line index gradients of S0 galaxies in Fornax cluster.

Name	Grad(Hβ*)	Grad(Fe5015*)	Grad(Mg$_1$)	Grad(Mg$_2$)	Grad(Mgb*)	Grad(Fe5270*)	Grad(Fe5335*)	Grad(Fe5406*)	Grad(Fe5709*)	Grad(Fe5782*)
(1)	(2)	(3)	(4)	(5)	(6)	(7)	(8)	(9)	(10)	(11)
NGC 1316	−0.012 (0.007)	**−0.030 (0.010)**	**−0.008 (0.002)**	**−0.036 (0.003)**	**−0.048 (0.008)**	**−0.049 (0.011)**	−0.037 (0.016)	−0.011 (0.011)	−0.004 (0.004)	−0.002 (0.010)
NGC 1380	0.009 (0.005)	−0.011 (0.008)	**−0.026 (0.002)**	**−0.043 (0.003)**	**−0.060 (0.007)**	−0.013 (0.008)	0.001 (0.013)	−0.012 (0.009)	−0.004 (0.003)	−0.018 (0.009)
NGC 1381	0.005 (0.005)	0.008 (0.005)	−0.016 (0.006)	**−0.025 (0.002)**	**−0.045 (0.005)**	−0.012 (0.007)	0.003 (0.011)	0.010 (0.008)	−0.002 (0.003)	0.010 (0.007)
NGC 1380A	**−0.026 (0.007)**	−0.014 (0.009)	−0.004 (0.002)	−0.006 (0.003)	−0.004 (0.007)	−0.011 (0.010)	−0.008 (0.015)	−0.010 (0.011)	0.003 (0.004)	−0.008 (0.010)
NGC 1375	**−0.061 (0.010)**	**−0.058 (0.012)**	−0.001 (0.003)	**−0.020 (0.004)**	0.005 (0.010)	**−0.042 (0.014)**	**−0.075 (0.022)**	−0.046 (0.016)	0.005 (0.006)	−0.019 (0.015)
IC 1963	−0.013 (0.006)	0.015 (0.009)	0.000 (0.005)	−0.002 (0.003)	−0.001 (0.007)	0.006 (0.010)	0.008 (0.016)	0.011 (0.010)	0.002 (0.004)	−0.001 (0.009)
ESO 358-G059	−0.020 (0.035)	0.013 (0.047)	0.018 (0.014)	−0.024 (0.013)	−0.073 (0.037)	−0.026 (0.051)	−0.086 (0.081)	0.020 (0.058)	0.009 (0.021)	−0.047 (0.050)
ESO 358-G006	0.003 (0.011)	0.014 (0.019)	**0.047 (0.000)**	0.018 (0.070)	0.000 (0.013)	0.012 (0.018)	−0.011 (0.028)	0.006 (0.019)	0.005 (0.007)	−0.003 (0.017)
ESO 359-G002	**−0.138 (0.031)**	−0.021 (0.039)	−0.015 (0.010)	**0.044 (0.012)**	**0.097 (0.032)**	**0.104 (0.046)**	−0.018 (0.073)	0.005 (0.048)	0.006 (0.019)	−0.029 (0.049)

Note. From (2) to (11), 1σ rms errors between '( )'; Col. (1), galaxy name; Col. (2), Hβ index; Col. (3), Fe5015 index; Col. (4), Mg$_1$ index in magnitudes; Col. (5), Mg$_2$ index in magnitudes; Col. (6), Mgb index; Col. (7), Fe5270 index; Col. (8), Fe5335 index; Col. (9), Fe5406 index; Col. (10), Fe5709 index; Col. (11), Fe5782 index. Gradients calculated with line indices in magnitudes (Paper III) with respect to log($R/R_{\rm HALF}$) (radii normalized by the half-light radius of each galaxy). Significant gradients ($\geq$3σ detections) are highlighted in bold.

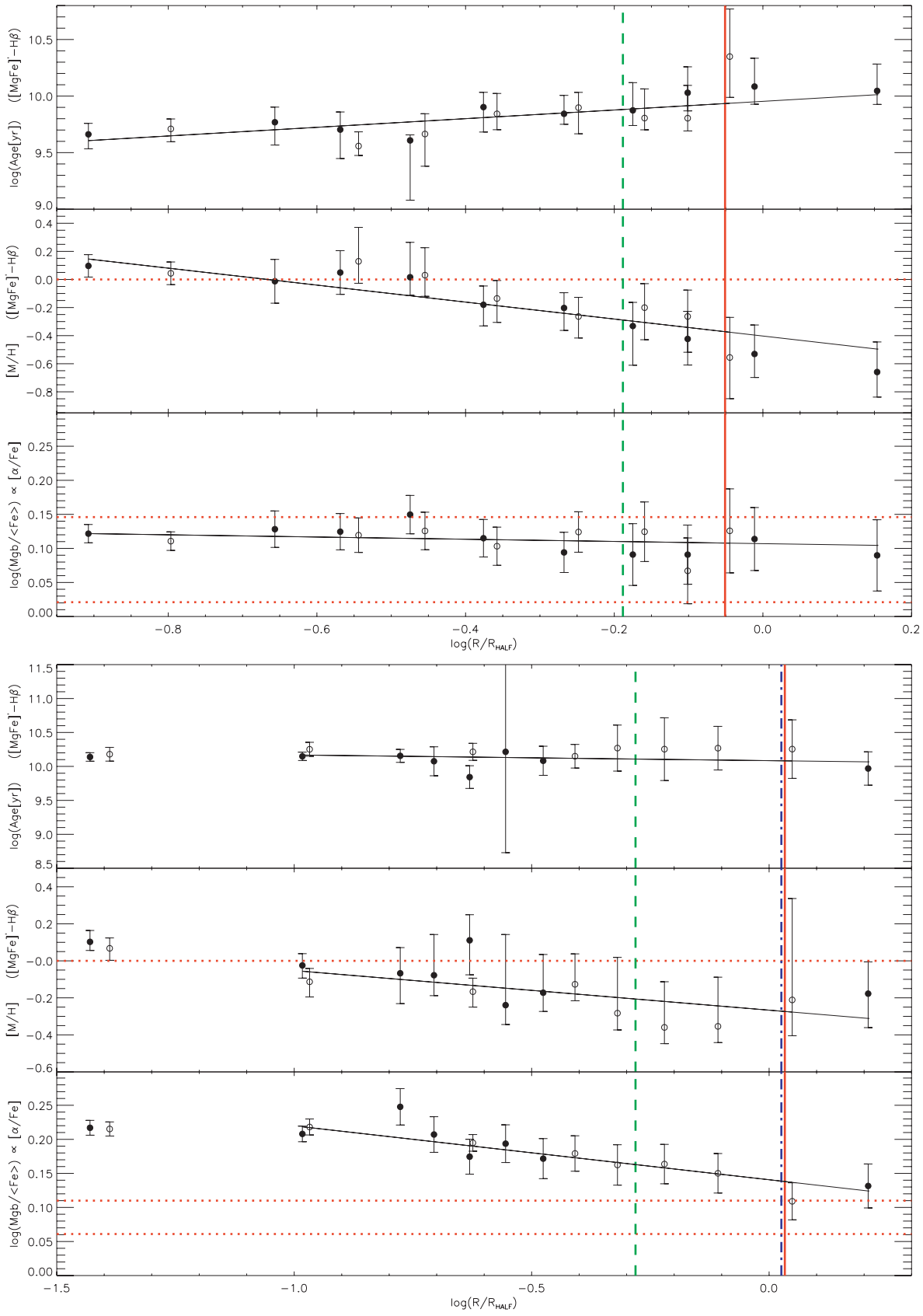

Figure B1. Gradients along the semimajor axis of NGC 1316 (top) and NGC 1380 (bottom), including predicted Ages, Metallicities and α-element tracer values. Filled (open) symbols correspond to: SW (NE) (for NGC 1316) and S (N) (for NGC 1380). The description of the different lines can be found in the text.

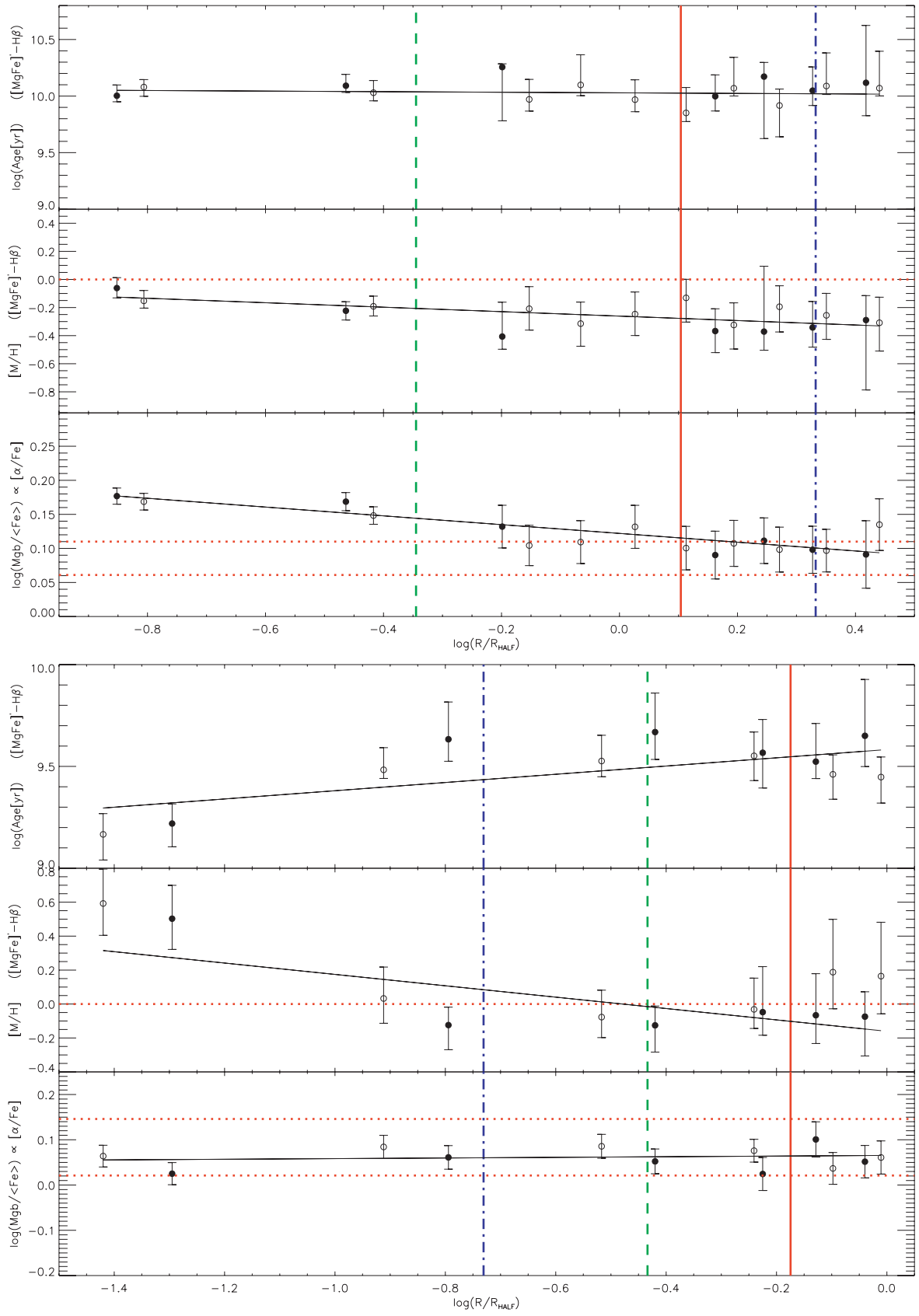

Figure B2. Same as Fig. B1 for NGC 1381 (top) and NGC 1380A (bottom). Filled (open) symbols correspond to: SE (NW) (for NGC 1381) and S (N) (for NGC 1380A).

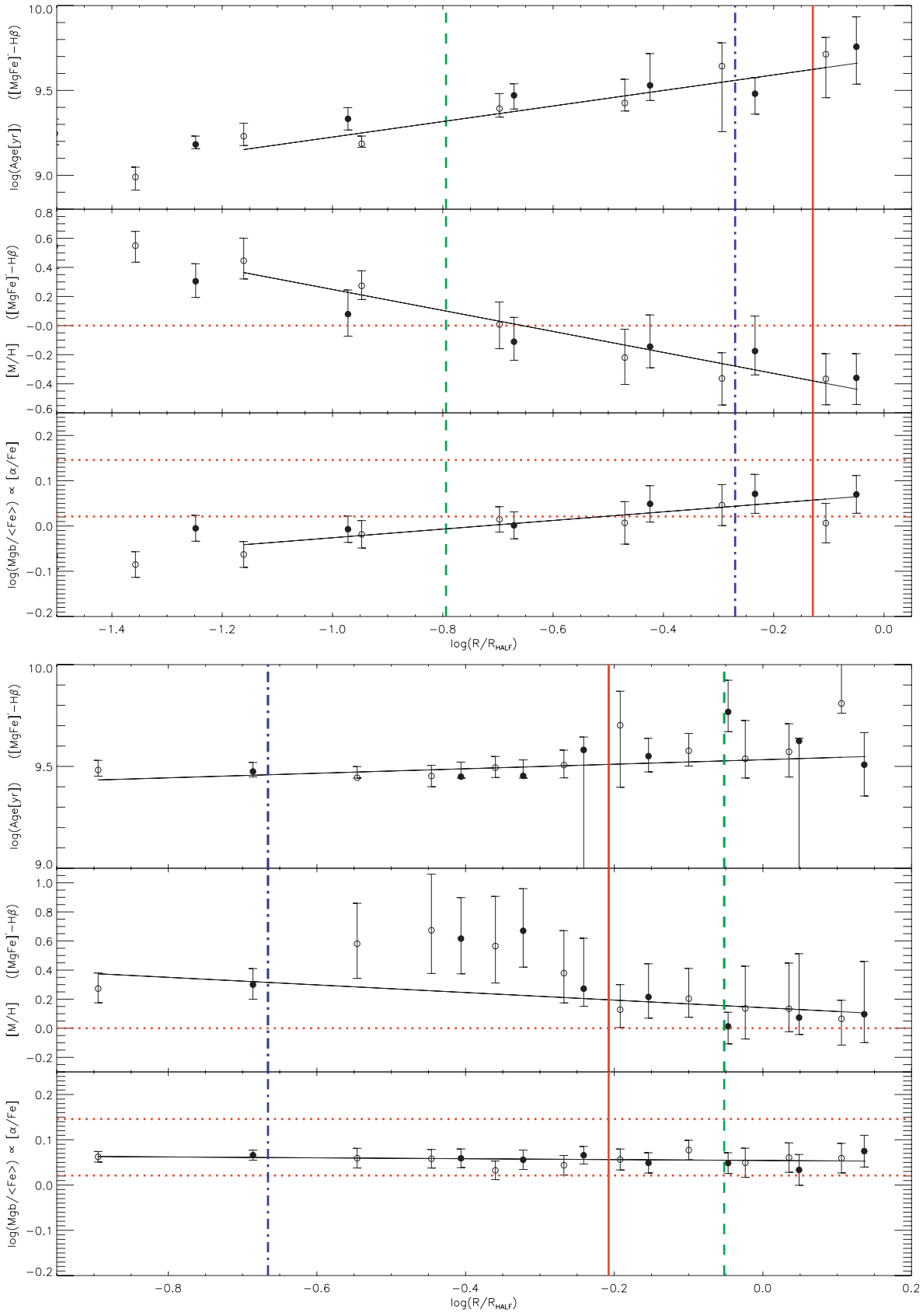

Figure B3. Same as Fig. B1 for NGC 1375 (top) and IC 1963 (bottom). Filled (open) symbols correspond to: the W (E) profile projected in the sky (for both galaxies).

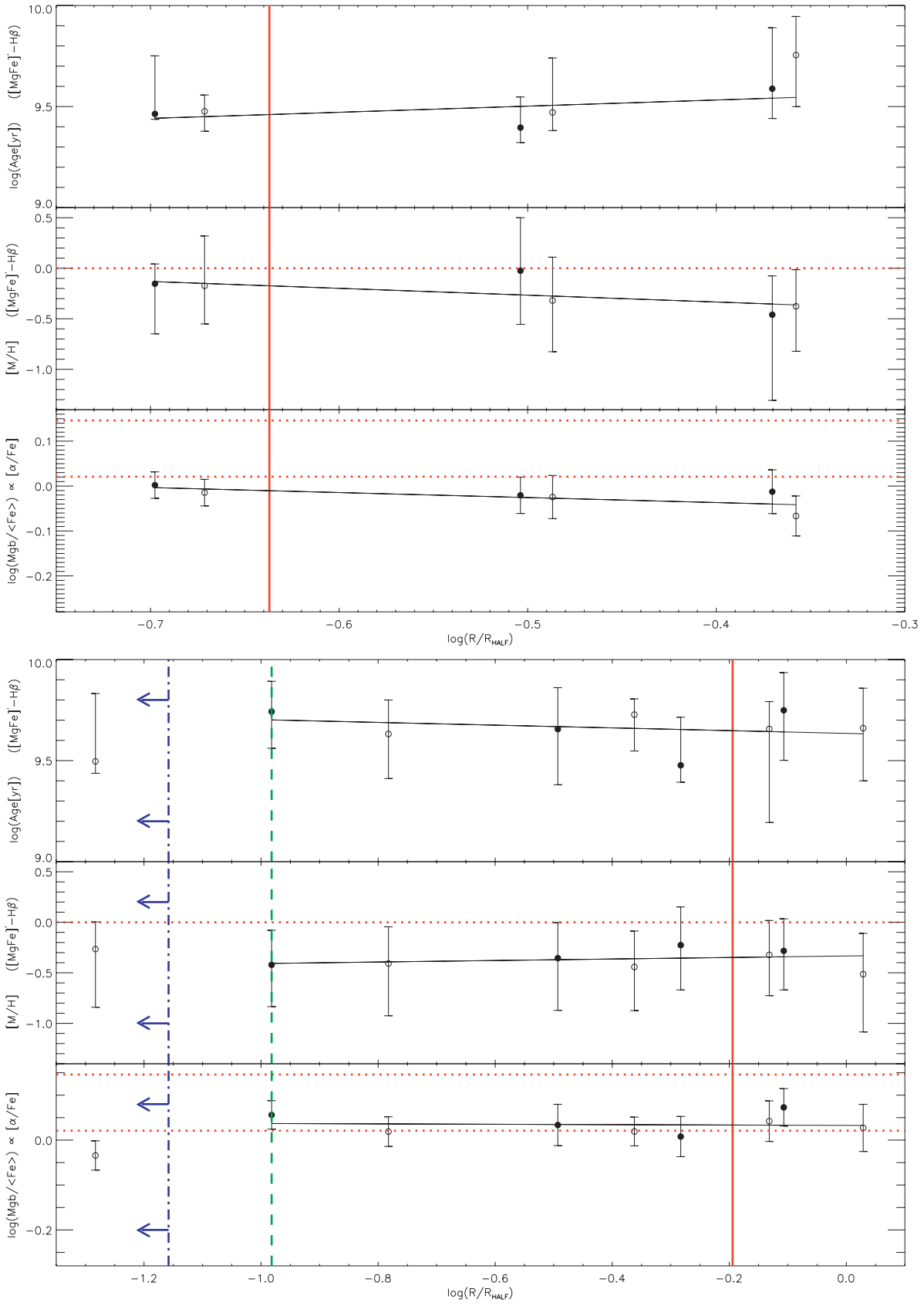

Figure B4. Same as Fig. B1 for ESO 358-G059 (top) and ESO 358-G006 (bottom). Filled (open) symbols correspond to the SE (NW) (for ESO 358-G059) and SW (NE) (for ESO 358-G006).

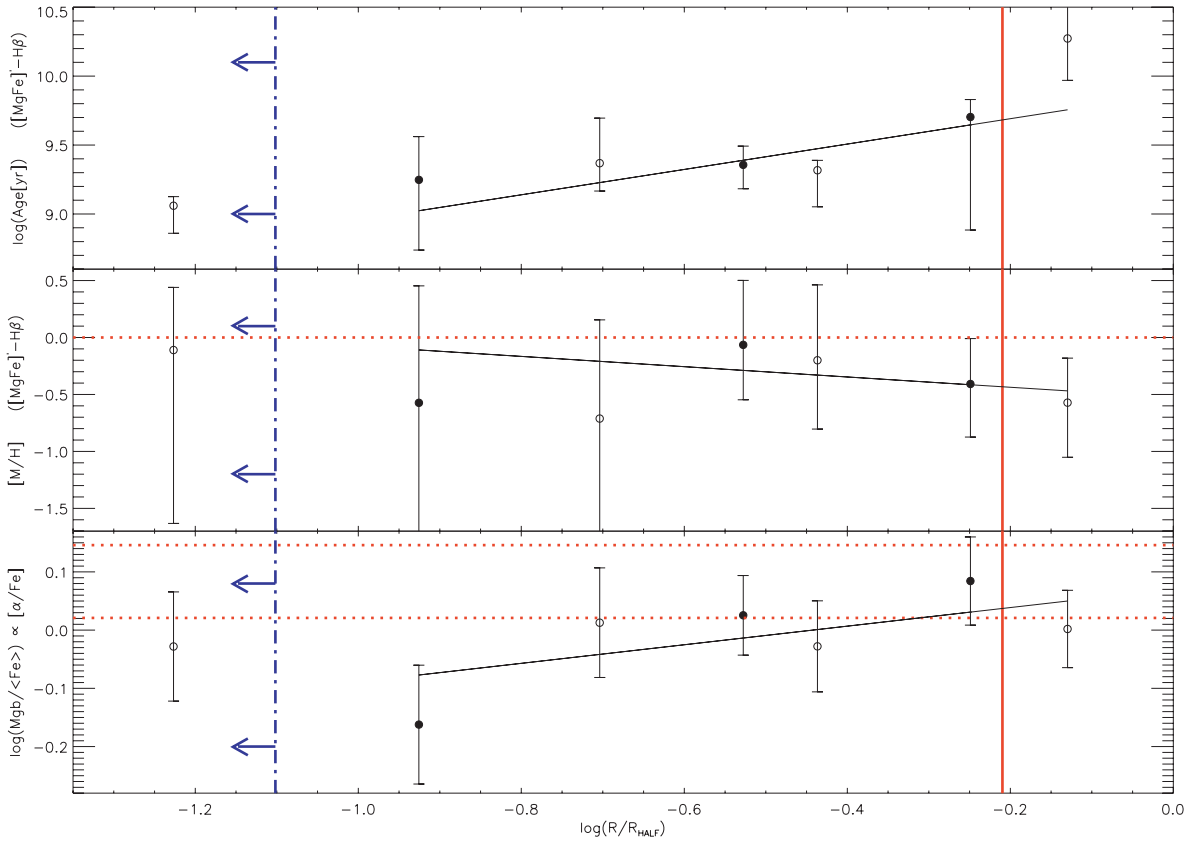

Figure B5. Same as Fig. B1 for ESO 359-G002. Filled (open) symbols correspond to the SW (NE) profile projected in the sky.

Table B1. Age, [M/H] and Mg*b*/⟨Fe⟩ gradients in Fornax S0s.

Name (1)	Grad(log Age[yr]) (2)	Grad[M/H] (3)	Grad(α) (4)
NGC 1316	$0.38^{+0.14}_{-0.13}$	$\mathbf{-0.60}^{+0.15}_{-0.10}$	−0.02 (0.02)
NGC 1380	$-0.08^{+0.09}_{-0.14}$	$-0.21^{+0.18}_{-0.03}$	**−0.08 (0.02)**
NGC 1381	$-0.03^{+0.07}_{-0.10}$	$-0.16^{+0.10}_{-0.04}$	**−0.07 (0.01)**
NGC 1380A	$0.20^{+0.13}_{-0.08}$	$-0.34^{+0.14}_{-0.11}$	0.01 (0.02)
NGC 1375	$0.46^{+0.31}_{-0.04}$	$\mathbf{-0.72}^{+0.12}_{-0.18}$	**0.10 (0.03)**
IC 1963	$0.11^{+0.09}_{-0.12}$	$-0.26^{+0.14}_{-0.12}$	−0.01 (0.02)
ESO 358-G059	$0.30^{+0.65}_{-0.64}$	$-0.68^{+1.45}_{-1.78}$	−0.11 (0.11)
ESO 358-G006	$-0.07^{+0.24}_{-0.20}$	$0.08^{+0.51}_{-0.51}$	−0.00 (0.04)
ESO 359-G002	$0.92^{+0.41}_{-0.54}$	$-0.45^{+1.23}_{-0.96}$	0.16 (0.13)

Note. For (2) and (3), asymmetric 1σ rms uncertainties included; For (4), 1σ rms errors between parentheses; Cols (2) and (3): SSP age and [M/H] from Hβ versus [MgFe]' diagram; Col. (4): gradient in log(Mg*b*/⟨Fe⟩) as an α-abundance tracer. Significant gradients ($\geq$3σ detections) are highlighted in bold.

This paper has been typeset from a TEX/LATEX file prepared by the author.